separations

MDPI

Article

Sponge-like Modified White-Rot Fungi Adsorbent for Rapid Removal of Pb(II) and Cd(II) from Solution: Selective Performance and Mechanistic Insights

Chunxiao Wang [1,†], Zhirong Chen [1,†], Nana Wang [1,*], Jianqiao Wang [1], Runshen He [1], Yu Chen [1], Haerfosai Nuhu [1], Hang Chen [1], Zhixuan Lin [1], Minqi Fan [1] and Mingdong Chang [2,*]

[1] School of Environmental Science and Engineering, Guangzhou University, Guangzhou 510006, China; cxwang2025@126.com (C.W.); zrchen85881@126.com (Z.C.); wangjq@gzhu.edu.cn (J.W.); like20200818@163.com (R.H.); yuchen202505@126.com (Y.C.); haer1120@126.com (H.N.); hchen7777777@126.com (H.C.); zxlin2025@126.com (Z.L.); mqfan778877@126.com (M.F.)

[2] Key Laboratory for Water Quality and Conservation of the Pearl River Delta, Ministry of Education, Guangzhou 510006, China

* Correspondence: nnwang@gzhu.edu.cn (N.W.); mdchang@gzhu.edu.cn (M.C.); Tel./Fax: +86-20-3934-1629 (N.W.)

† These authors contributed equally to this work.

Abstract

Heavy metal pollution, especially from Pb(II) and Cd(II), poses significant risks due to its persistence and bioaccumulation potential. Traditional removal methods face challenges like high costs and secondary pollution. This study developed a novel three-dimensional porous adsorbent XBS, derived from xanthate-modified *Phanerochaete sordida* YK-624 (a white-rot fungus), for the rapid and efficient removal of Pb(II) and Cd(II) from wastewater. Characterization showed that XBS has a sponge-like structure with abundant functional groups, significantly enhancing its adsorption capacity and kinetics. XBS achieved 96% Pb(II) and 32% Cd(II) removal within 1 min at a 0.25 g/L dose, reaching over 95% of the maximum adsorption capacity within 30 min for Pb(II) and 240 min for Cd(II). The maximum capacities were 224.72 mg/g for Pb(II) and 82.99 mg/g for Cd(II). Kinetic and thermodynamic analyses indicated a chemisorption-driven process, which was both endothermic and spontaneous. XBS exhibited high selectivity for Pb(II) over Cd(II) and other metals (Tl(I), Cu(II)), attributed to stronger covalent interactions with sulfur- and nitrogen-containing groups. Mechanistic analyses (XRD, FTIR, and XPS) revealed that removal occurs via ion exchange, complexation, and precipitation, forming stable compounds like PbS/CdS and $PbCO_3$/$CdCO_3$. Given its cost-effectiveness, scalability, and high efficiency, XBS represents a promising adsorbent for heavy metal remediation, particularly in Pb(II)-contaminated wastewater treatment applications.

Keywords: heavy metal; white-rot fungi; adsorption behavior; selectivity; removal mechanism

check for updates

Academic Editor: Grzegorz Boczkaj

Received: 15 May 2025
Revised: 21 June 2025
Accepted: 26 June 2025
Published: 28 June 2025

Citation: Wang, C.; Chen, Z.; Wang, N.; Wang, J.; He, R.; Chen, Y.; Nuhu, H.; Chen, H.; Lin, Z.; Fan, M.; et al. Sponge-like Modified White-Rot Fungi Adsorbent for Rapid Removal of Pb(II) and Cd(II) from Solution: Selective Performance and Mechanistic Insights. *Separations* **2025**, *12*, 172. https://doi.org/10.3390/separations12070172

Copyright: © 2025 by the authors. Licensee MDPI, Basel, Switzerland. This article is an open access article distributed under the terms and conditions of the Creative Commons Attribution (CC BY) license (https://creativecommons.org/licenses/by/4.0/).

1. Introduction

Heavy metal ions, due to their non-degradability, bioaccumulation, and persistence can enter food chains through various pathways and accumulate in organisms, resulting in severe environmental and human health risks [1,2]—especially lead and cadmium [3,4]. With rapid industrial development, wastewater discharges containing Pb(II) and Cd(II)

from mining, metallurgy, electroplating, and chemical industries have increased continuously. Given their environmental persistence, the effective removal of these toxic metals from water has become a global priority. Current technologies, such as chemical precipitation, membrane separation, electrochemical treatment, and biological treatment, often suffer from high costs, inefficiency, and the risk of secondary pollution [5]. Consequently, research has increasingly focused on adsorption, which is considered the most promising method for removing heavy metal ions from solutions due to its cost-effectiveness, operational simplicity, high efficiency, and flexibility [6]. However, traditional adsorbents are limited by low adsorption capacities and complex procedures, particularly for rapid removal. Therefore, the key challenges lie in developing adsorbents with high adsorption capacities, and simplified operational processes for efficient Pb(II) and Cd(II) removal.

The design of effective adsorbents for heavy metal removal requires careful consideration of multiple performance criteria, including low cost, high adsorption capacity, rapid adsorption kinetics, ease of operation, and large-scale application potential. Chemisorption-based materials, which rely on specific interactions between functional groups and target metal ions, often employ chemical modifications to increase active site density [7]. However, such modifications frequently involve complex synthetic procedures that elevate production costs and technical challenges. The adsorption process itself occurs through three consecutive steps: (1) mass transfer from bulk solution to the adsorbent surface, (2) surface binding at active sites, and (3) intra-particle diffusion to interior adsorption sites [5]. Optimal adsorbent performance depends critically on efficient intraparticle diffusion and subsequent interactions with functional groups, which collectively determine both adsorption rates and the ultimate metal uptake capacity. While nanostructured adsorbents offer potential advantages through enhanced surface area and reduced diffusion path lengths, practical limitations include particle agglomeration [8,9] and challenging solid–liquid separation requirements. Meanwhile, fine particulate adsorbents often prove unsuitable for continuous-flow systems due to excessive pressure drops and material loss. These limitations can be overcome through developing three-dimensional porous adsorbents with hierarchical pore structures. These structures combine macropores of various sizes for rapid mass transport and a high surface area, along with numerous accessible functional groups for effective metal binding. Such engineered materials embody an optimal balance between performance and practicality for water treatment applications.

Recently, low-cost biomaterials have garnered significant attention for their potential to remove toxic metal ions from solutions [10–15]. Particular fungal species, including *Trichoderma brevicompactum* [16] and *Aspergillus niger* [17], exhibit exceptional metal-binding capacities due to their cell wall composition being rich in proteins and polysaccharides containing various reactive functional groups (-OH, -NH_2, and -COOH) that facilitate effective metal complexation [18]. Among various fungal species, white-rot fungi have emerged as particularly promising candidates for heavy metal removal, offering broad prospects due to their natural abundance, environmental ubiquity, and cost-effectiveness [19,20]. White-rot fungi are particularly abundant in forest ecosystems, where they play a vital role in lignin decomposition and organic matter cycling [21]. These fungi employ multiple metal removal mechanisms including cell wall adsorption, the enzymatic alteration of metal valence states, and extracellular polymeric substance (EPS) sequestration [22]. However, while living white-rot fungal systems show potential, their practical application is limited by sensitivity to high metal concentrations and environmental fluctuations [23,24]. In contrast, inactivated (non-living) fungal biomass demonstrates superior metal removal capacity, as it is unaffected by toxicity and more amenable to chemical modification for performance enhancement [25]. Although modified fungal biosorbents have achieved improved Pb(II) removal capabilities [26,27], their adsorption performance remains suboptimal for practical

applications. We found that among various chemical modification methods, xanthation modification is a promising one. It can form insoluble xanthate groups (-C(=S)-S-Na), which have a strong complexing ability for heavy metal ions [28]. Therefore, we propose developing chemically modified fungal materials with three-dimensional network structures, designed to achieve both rapid adsorption kinetics and facile separation properties.

According to the hard and soft acids and bases theory, Pb(II) and Cd(II) are classified as borderline acids or Lewis soft acids [29], exhibiting a strong affinity for Lewis soft-base functional groups such as -NH_2, -NH, and -C(=S)-S- functional groups [30]. This chemical compatibility forms the theoretical foundation for xanthate modification, which introduces the -C(=S)-S- chelating group through a base-catalyzed reaction between fungal hydroxyl groups and carbon disulfide (CS_2), as illustrated in Equation (1).

$$\text{R–OH} + CS_2 + \text{NaOH} \rightarrow \text{R–OC(=S)SNa} \quad (1)$$

This modification not only introduces metal-chelating functional groups but also imparts hydrogel-like properties that facilitate the formation of three-dimensional network structures [31]. White-rot fungi serve as ideal substrates for xanthate modification due to their high content of hydroxyl functional groups and existing amino/carboxyl groups for synergistic metal binding. However, it remains unclear whether white-rot fungi can be successfully modified into a porous adsorbent with a three-dimensional network structure that offers rapid adsorption kinetics, high adsorption capacity, and easy solid–liquid separation, and whether it can overcome the batch-to-batch variability inherent in biological substrates.

This study proposes that functionalization driven by CS_2 can effectively transform white-rot fungi into a three-dimensional porous adsorbent through a straightforward one-pot modification process, facilitating the efficient removal of Pb(II) and Cd(II) from aqueous solutions. The central hypothesis suggests that the xanthation reaction will concurrently: (1) introduce -C(=S)-S- chelating groups with a high affinity for heavy metal ions, and (2) promote the formation of an interconnected macroporous network structure that is conducive to rapid mass transfer. To systematically evaluate this hypothesis, the investigation includes five specific objectives: (1) assess the impact of CS_2-driven functionalization on white-rot fungi and characterize its textural properties; (2) achieve the rapid removal of Pb(II) and Cd(II) ions, even at trace concentrations; (3) examine the adsorption behaviors of modified white-rot fungi for Pb(II) and Cd(II) under various environmental conditions; (4) evaluate the selective adsorption of Pb(II) and Cd(II) ions in the presence of other heavy metals; and (5) investigate the mechanisms behind Pb(II) and Cd(II) adsorption.

2. Materials and Methods

2.1. Microorganisms and Chemicals

The white-rot fungus strain *Phanerochaete sordida* YK-624 (American Type Culture Collection 90872) used in this experiment was purchased from the United States Culture Center. *P. sordida* YK-624 (denoted as YK) was cultured aerobically on sterilized potato dextrose agar (PDA) slants at 30 °C for 3 d. For biomass production, the culture was homogenized using a tissue disrupter and subsequently inoculated into sterilized potato dextrose broth (PDB) medium for 5 d of submerged cultivation at 30 °C with continuous shaking (120 rpm). Fungal biomass was harvested during mid-exponential growth phase by centrifugation, followed by repeated washing with deionized water. The collected YK was subsequently freeze-dried and ground into powder, which served as the raw material for the modified adsorbent used later in the experiment.

Lead nitrate ($Pb(NO_3)_2$) and cadmium nitrate ($Cd(NO_3)_2{\cdot}4H_2O$) were obtained from Shanghai Macklin Biochemical Co., Ltd. (Shanghai, China), while Pb and Cd standard

solutions were sourced from Aladdin Industrial Corporation (Shanghai, China). Sodium hydroxide (NaOH) and carbon disulfide (CS_2), used for the xanthate reaction, were purchased from Sinopharm Chemical Reagent Co., Ltd. (Shanghai, China) and Macklin Biochemical Co., Ltd. (Shanghai, China), respectively. HCl and HNO_3 were supplied by Guangzhou Chemical Reagent Factory. All chemical reagents used in the experiment were of analytical grade and were used without further purification. Deionized water (resistivity >18 MΩ·cm) from a Millipore Milli-Q purification system was used throughout the experiments.

2.2. Preparation of Modified Adsorbent

The white-rot fungus-modified adsorbent was prepared using a straightforward one-step method. To summarize, 0.50 g of inactivated YK powder (dry weight) was combined with 37.5 mL of a 14 wt% NaOH solution and 2.0 mL of carbon disulfide (CS_2). The mixture was stirred continuously at 25 °C for 3 h to ensure complete xanthation. Following the reaction, the product was collected by centrifugation and washed with ultrapure water until the supernatant achieved a neutral pH. The resulting gel-like product was then freeze-dried, yielding the porous modified fungus adsorbent, designated as XBS. The preparation flowchart is depicted in Figure 1.

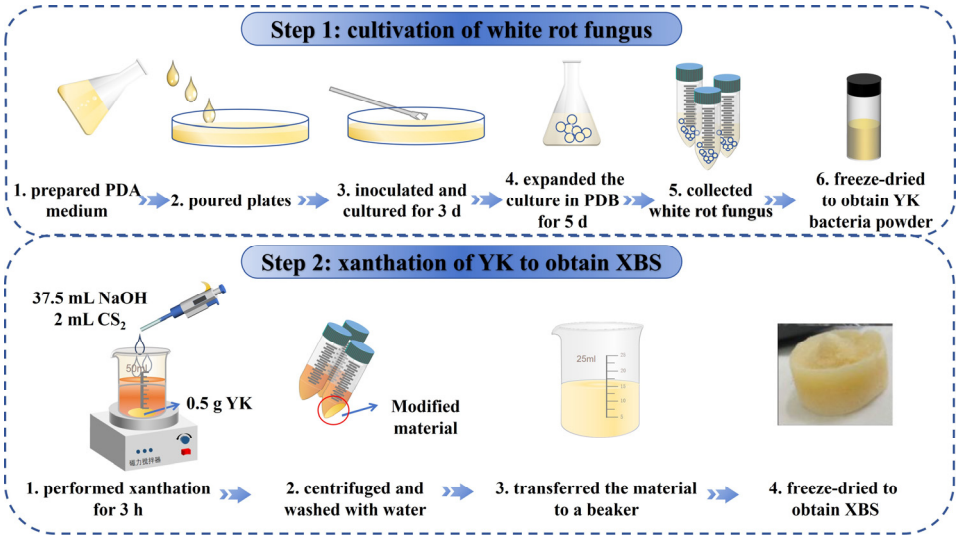


Figure 1. The preparation flow chart of XBS.

2.3. Batch Adsorption Experiments

The adsorption behaviors of XBS for Pb(II) and Cd(II) were systematically investigated through batch experiments conducted in 50 mL polypropylene conical tubes containing 0.20 g/L XBS and 50 mg/L metal solutions, with agitation at 200 rpm (at 25 ± 0.5 °C) for 720 min. pH optimization studies were performed across ranges of 2–5 (for Pb(II)) and 2–6 (for Cd(II)) using 0.1 M HNO_3/NaOH adjustments, with the optimal pH selected for subsequent tests. Adsorption kinetics experiments were conducted with initial Pb(II) and Cd(II) concentrations of 10 and 50 mg/L, measuring at sampling intervals from 0.08 to 720 min, respectively. Adsorption isotherms were evaluated using initial concentrations ranging from 5 to 200 mg/L at temperatures of 25 °C, 35 °C, and 45 °C for 720 min each. Competitive adsorption was assessed in binary systems (Pb(II)/Cd(II) with Tl(I)/Cu(II)/Cd(II)/Pb(II)) at molar ratios of 1:1 to 2:1 (0.1 to 2.0 mmol/L).

After the adsorption reactions, all samples were filtered using a 0.22 μm filtration membrane, and the residual concentrations of heavy metal ions in the post-adsorption solutions were determined via atomic absorption spectroscopy (AAS, 900T, PerkinElmer Co., Waltham, MA, USA). All batch experiments were repeated in triplicate, and the average

value of the parallel samples was used to analyze adsorption behaviors. The adsorption capacity (q, mg/g) and removal rate (R, %) of XBS for heavy metal ions were calculated using the following equations:

$$q = \frac{(c_0 - c_e) \times V}{m} \quad (2)$$

$$R = \frac{c_0 - c_e}{c_0} \times 100\% \quad (3)$$

where c_0 and c_e (mg/L) represent the initial and equilibrium concentrations of the heavy metal ions in the solution, respectively, V (L) is the solution volume, and m (g) is the mass of XBS.

2.4. Characterization

The physicochemical properties of XBS, both before and after adsorption, were comprehensively characterized using multiple analytical techniques. Microstructural changes in XBS were observed via cold field-emission scanning electron microscopy (SEM, S4800, Hitachi Co., Tokyo, Japan). The specific surface areas were measured using an ASAP 2460 adsorption analyzer (Micromeritics Co., Norcross, GA, USA) via nitrogen adsorption–desorption isotherms, employing the Brunauer–Emmett–Teller (BET) theory. The crystalline structures of XBS before and after adsorption were analyzed using an X-ray diffractometer (XRD, D/max-2500, Rigaku, Tokyo, Japan) with Cu Kα radiation (λ = 1.5406 Å) at 4°/min scanning rate over 5–80° 2θ range. Changes in the organic functional groups on the surface of XBS were characterized using Fourier transform infrared spectroscopy (FTIR, Tensor 27, Bruker Co., Karlsruhe, BW, Germany) using KBr pellets across the range of 500–4000 cm^{-1} at room temperature. Additionally, surface chemistry properties were examined through X-ray photoelectron spectroscopy (XPS, Escalab 250Xi, Thermo Fisher Scientific Co., Waltham, MA, USA) using monochromatic Al Kα radiation, where all spectra were charge-corrected using the adventitious carbon C1s peak at 284.8 eV as an internal reference. For post-adsorption samples, careful washing with deionized water followed by freeze-drying was conducted prior to all analyses to ensure the removal of non-specifically bound metal ions while preserving the adsorption complexes.

2.5. Regeneration and Reusability Studies

The regeneration capacity and reusability of XBS were systematically evaluated through three consecutive adsorption–desorption cycles. For Pb(II) adsorption, experiments were conducted under optimized conditions: an initial concentration of 50 mg/L, an adsorbent dosage of 0.2 g/L, pH 5.0, and a contact time of 360 min. Corresponding Cd(II) adsorption studies utilized the same dosage and concentration but at pH 6.0 and a contact time of 480 min. Following each adsorption cycle, XBS loaded with Pb(II) or Cd(II) was subjected to elution using 0.5 M HNO_3 and 0.5 M HCl solutions. The desorbed adsorbent was then thoroughly rinsed with deionized water until a neutral pH was achieved and subsequently reused for the next adsorption cycle under identical conditions. This sequential process was repeated for three complete cycles to assess the stability and regeneration efficiency of XBS, with the metal removal efficiency and adsorption capacity being measured after each cycle to evaluate the performance degradation.

3. Results and Discussion

3.1. Morphological Structural Characteristics

The transformation from native white-rot fungus powder to XBS adsorbent represents a significant morphological advancement, as clearly evidenced in Figure 2. While the unmodified fungal biomass exists as irregular agglomerates of disordered, branch-like

rods with minimal structural organization (Figure 2a,b), the modified XBS develops a highly organized three-dimensional macroporous architecture, where interwoven fibrous structures form a sponge-like network with densely distributed pores of varying sizes and the fiber surfaces exhibit rough textures and uneven topographies (Figure 2c,d). This hierarchical structure ensures a high surface-to-volume ratio, which is critical for maximizing adsorption capacity. Simultaneously, the interconnected pores between fibers provide a low-resistance pathway for the diffusion of heavy metal ions. Nitrogen physisorption analysis (Figure S1) quantitatively confirms these structural enhancements, showing a Type II isotherm characteristic of macroporous materials with a 5.6-fold increase in specific surface area (3.63 m^2/g vs. 0.65 m^2/g for native fungus) and a total pore volume of 0.004310 cm^3/g, consistent with high-performance fungal-derived adsorbents reported in the literature [32,33]. The lyophilization process, through controlled ice crystal formation and subsequent sublimation, simultaneously engineers this hierarchical porosity while imparting exceptional hydrophilicity to the material. This hierarchical pore structure significantly enhances wastewater treatment performance by enabling efficient solid–liquid separation and facilitating rapid heavy metal adsorption through shortened intra-particle diffusion pathways, while maximizing accessibility to the active functional groups distributed throughout the porous matrix [34], thus readily improving its adsorption efficiency. The combined advantages of macroporous transport pathways and newly-introduced active sites make XBS particularly suitable for practical wastewater treatment applications, addressing both adsorption capacity and separation efficiency requirements.

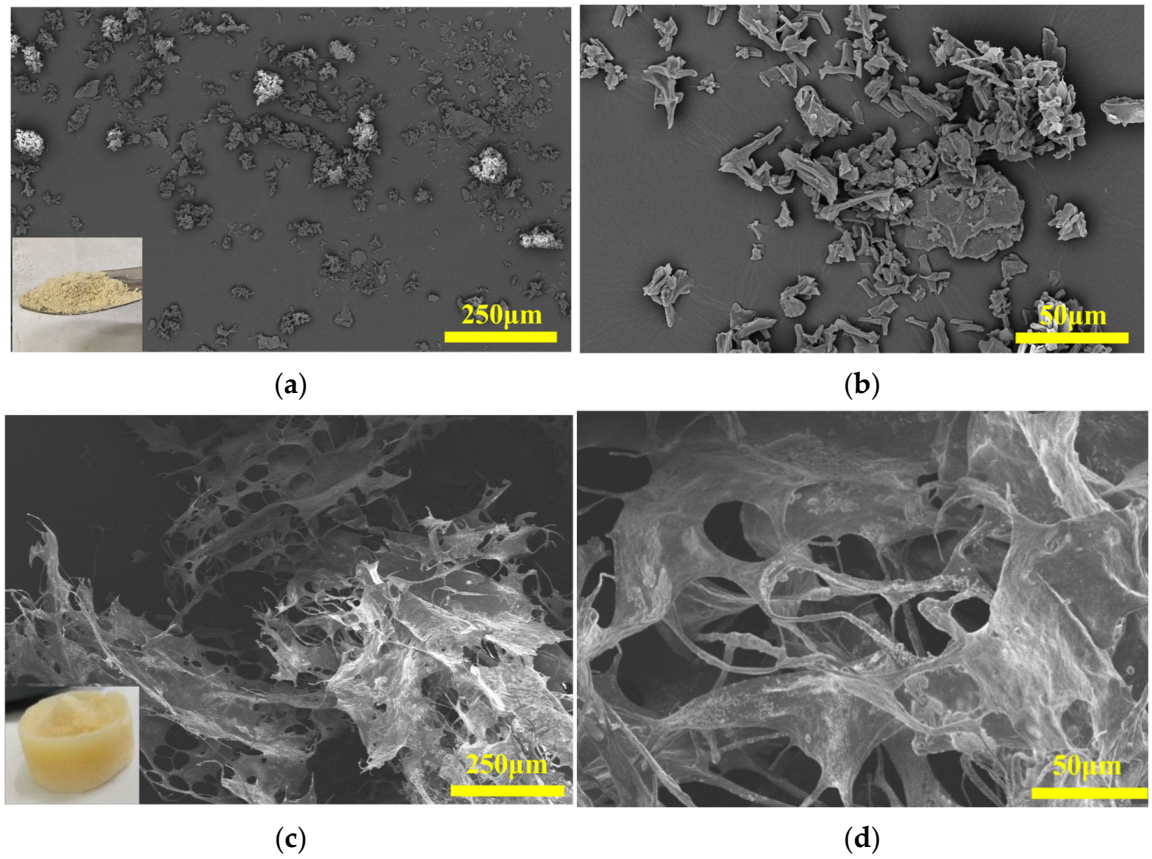


Figure 2. SEM images and appearance photographs of the original white-rot fungi (**a**,**b**) and XBS (**c**,**d**).

3.2. Pb(II) and Cd(II) Removal Performances of XBS

3.2.1. Effect of pH

Solution pH critically governs heavy metal adsorption efficiency by modulating both adsorbent surface chemistry and metal speciation. A systematic evaluation across pH 2–6 (avoiding precipitation regimes) revealed strong positive correlations between pH and Pb(II)/Cd(II) uptake by XBS (Figure 3a). This pH-dependence originates from three interconnected mechanisms: (1) Competitive proton effects dominate under highly acidic conditions (pH < 3), where high H^+ concentrations protonate key functional groups while competing with metal cations for binding sites. (2) Surface charge modulation, confirmed by zeta potential measurements (Figure 3b), reveals the adsorbent's point of zero charge (pzc) below pH 1.0, ensuring a negatively charged surface at operational pH conditions (5 for Pb(II) and 6 for Cd(II)) that enhances electrostatic attraction of cationic metal species. (3) The stability of the xanthate group is compromised as acidic conditions lead to ligand decomposition and a subsequent loss in adsorption capacity. These interconnected mechanisms produce distinct adsorption edges, with Pb(II) showing a 528% capacity increase from pH 3 to 5, while Cd(II) exhibits a 125% enhancement from pH 4 to 6. Optimal performance at mildly acidic conditions (pH 5–6) reflects a critical balance between the deprotonation of functional groups, metal ion solubility and xanthate stability, achieving maximal electrostatic contributions while maintaining ligand integrity, thereby enhancing adsorption efficiency. This comprehensive understanding of pH effects allows for the precise operational control of XBS for efficient heavy metal removal across various wastewater compositions.

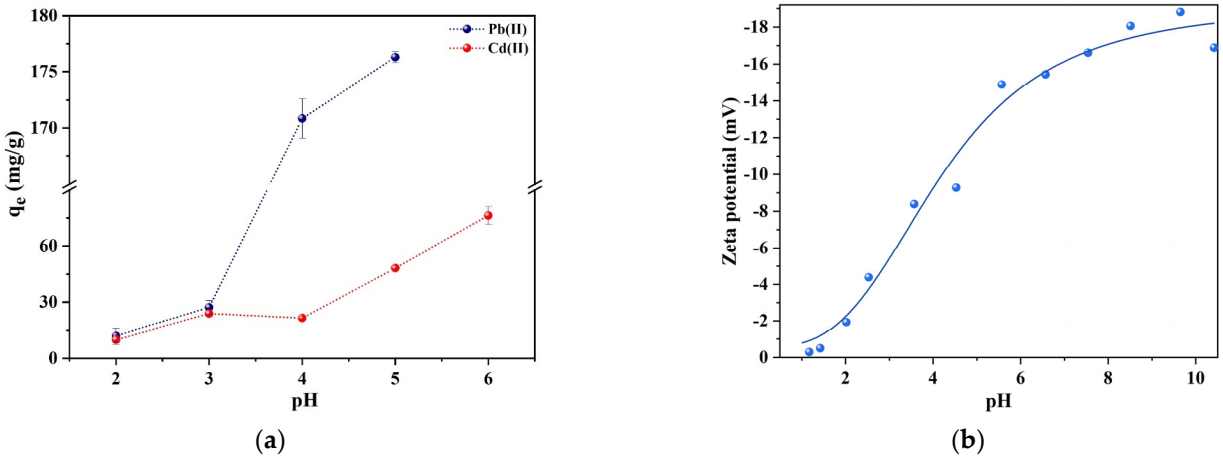
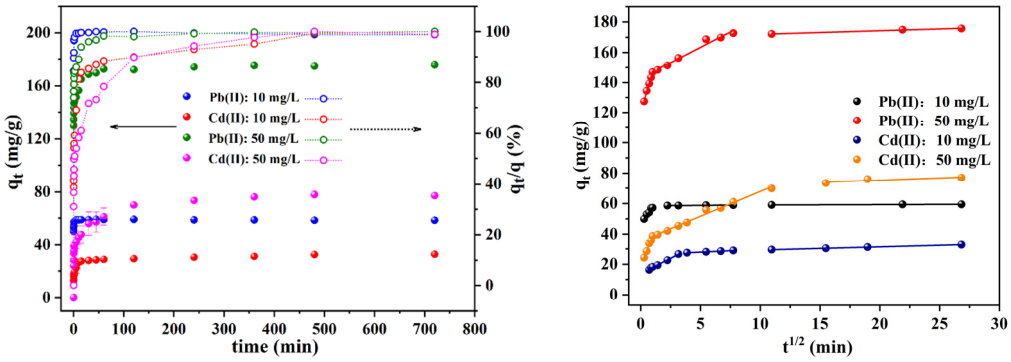


Figure 3. (**a**) Effect of solution pH on Pb(II) and Cd(II) adsorption by XBS and (**b**) the zeta potential of XBS.

3.2.2. Adsorption Kinetics

The effect of adsorption time on the removal of Pb(II) and Cd(II) by XBS at initial concentrations of 10 and 50 mg/L exhibit characteristic biphasic behavior (Figure 4a), comprising an initial rapid adsorption phase followed by gradual equilibrium attainment. This trend indicates that a substantial number of active sites on the XBS surface are readily accessible at the process's outset, resulting in swift adsorption. Nevertheless, as these sites become occupied, the number of remaining available sites diminishes, decelerating the adsorption rate until equilibrium is established. For solutions with a concentration of 10 mg/L, Pb(II) achieves a removal rate of 91% (accounting for 92% of the equilibrium adsorption capacity) within 30 s, significantly outperforming Cd(II), which only reaches a removal rate of 29% (50% of the equilibrium adsorption capacity). The kinetic disparity becomes more pronounced at higher concentrations (50 mg/L), while the adsorption

capacity for Pb(II) on XBS increases rapidly within 1 min, whereas for Cd(II), it increases over the initial 60 min. Equilibrium is attained at approximately 30 min for Pb(II) and 240 min for Cd(II) ($q_t/q \geq 95\%$), with equilibrium adsorption amounts of 175.75 mg/g for Pb(II) and 77.90 mg/g for Cd(II). The observed kinetic differences stem from fundamental variations in the metals' physicochemical properties: Pb(II) exhibits superior adsorption characteristics due to its higher electronegativity (2.33 vs. 1.69 for Cd(II)), stronger binding strength (logK = 2.68 vs. 2.15), and smaller hydrated radius (4.01 Å vs. 4.26 Å), which collectively enhance both diffusion kinetics and surface complexation efficiency [35,36]. Notably, XBS demonstrates significantly improved adsorption capacities compared to the unmodified YK material, with 88% and 102% increases for Pb(II) (175.75 vs. 93.39 mg/g) and Cd(II) (77.90 vs. 38.53 mg/g), respectively. The adsorption kinetics are governed by the combination of rapid surface complexation at readily accessible sites followed by slower intra-particle diffusion, with the hierarchical pore structure of XBS facilitating efficient mass transfer while maintaining abundant binding sites throughout the porous network [37].



(**a**) (**b**)

Figure 4. (**a**) Effect of contact time on the adsorption amounts of Pb(II) and Cd(II) by XBS at initial concentrations of 10 and 50 mg/L, The solid arrow indicates q_t, whereas the dotted arrow denotes q_t/q, and (**b**) the corresponding intra-particle diffusion model fitting plot.

The adsorption process occurs through three consecutive stages: (1) external film diffusion, where metal ions migrate through the solution boundary layer to the adsorbent surface; (2) intra-particle diffusion through the macro/mesoporous network; and (3) the adsorption reaction stage, where the metal ions are adsorbed at active sites on the inner surface of the pores. The overall adsorption rate is dictated by the slowest stage, known as the rate-controlling step, which is crucial for optimizing adsorbent performance. Kinetic analysis reveals the Pb(II) and Cd(II) adsorption on XBS follows pseudo-second-order (PSO) kinetics ($R^2 > 0.999$, Figure S2 and Table 1), as evidenced by the close agreement between calculated ($q_{e,cal}$) and experimental ($q_{e,exp}$) equilibrium capacities. The PSO model fit confirms chemisorption as the dominant mechanism involving electron sharing/exchange with active functional groups. The low k_2 values ($k_2 < 0.049$ g/(mg min)) indicate a strong affinity of Pb(II) and Cd(II) for the active sites on XBS, as well as a rapid uptake process, confirming the high efficiency of XBS in removing Pb(II) and Cd(II).

Table 1. Adsorption kinetic parameters for the adsorption of Pb(II) and Cd(II) by XBS.

Heavy Metal Ion	C_0 (mg/L)	$q_{e,exp}$ (mg/g)	Pseudo-First-Order			Pseudo-Second-Order			Intra-Particle Diffusion								
			k_1 (1/ min)	$q_{e,cal}$ (mg/g)	R^2	k_2 (g/(mg min))	$q_{e,cal}$ (mg/g)	R^2	$k_{id,1}$ (mg/g $min^{-0.5}$)	$C_{id,1}$ (mg/g)	R^2	$k_{id,2}$ (mg/g $min^{-0.5}$)	$C_{id,2}$ (mg/g)	R^2	$k_{id,3}$ (mg/g $min^{-0.5}$)	$C_{id,3}$ (mg/g)	R^2
Pb(II)	10	59.04	0.001	1.89	0.104	0.049	59.03	0.999	10.42	47.19	0.967	0.064	58.44	0.999	0.025	58.78	0.908
	50	175.75	0.004	3.64	0.749	0.007	158.59	1.000	26.87	120.21	0.996	4.020	143.29	0.972	0.230	169.63	0.993
Cd(II)	10	32.75	0.003	2.78	0.807	0.008	32.52	0.999	3.80	14.13	0.978	0.460	25.43	0.954	0.210	27.20	1.000
	50	77.90	0.003	4.56	0.880	0.002	77.70	0.999	20.21	18.53	0.994	3.250	35.44	0.988	0.290	69.61	0.800

The experimental data were further analyzed using the intra-particle diffusion model, with results presented in Figure 4b and Table 1. The fitting curves exhibit three distinct linear segments that do not intersect the origin. This pattern suggests that mass transfer is not the primary rate-limiting factor, and intra-particle diffusion alone cannot solely govern the adsorption rate. The initial steep slope of these curves corresponds to a rapid adsorption phase, where Pb(II) and Cd(II) quickly diffuse to and occupy binding sites on the external surface of XBS. This phase is completed within 2 to 5 min at an initial concentration of 10 mg/L, and it can be completed even faster, within 1 to 2 min, at a concentration of 50 mg/L. Following this rapid surface adsorption, the curves transition to a gradual slope, reflecting the progressive diffusion of pollutants into the internal matrix of the biomass. This slower phase of intra-particle diffusion ultimately results in an equilibrium stage characterized by substantially diminished diffusion rates, underscoring the crucial role that intra-particle diffusion plays in establishing the adsorption rates of Pb(II) and Cd(II) on XBS. The observation that the fitting lines do not intersect the origin provides additional insight, indicating that boundary layer resistance influences the adsorption process, and that chemical adsorption is also significantly important in retaining Pb(II) and Cd(II).

3.2.3. Adsorption Isotherm and Thermodynamics

The equilibrium adsorption isotherms of Pb(II) and Cd(II) on XBS at 298, 308, and 318 K (Figure 5) exhibit typical Langmuir-type behavior, where adsorption capacities increase with rising concentration until reaching saturation. This concentration-dependent behavior is driven by enhanced mass transfer under stronger concentration gradients, though the rate of adsorption decreases as available sites become occupied. Notably, elevated temperatures from 298 to 318 K improved adsorption capacities by 5.90 mg/g for Pb(II) and 8.08 mg/g for Cd(II), attributable to: (1) stronger interactions between the heavy metal ions and XBS functional groups at higher temperatures, and (2) the elevated temperature accelerating the transport of heavy metal ions from the bulk solution to the surface-bound phase, resulting in a greater removal of Pb(II) and Cd(II) from the solution. The moderate temperature sensitivity demonstrates XBS's robust performance across varying thermal conditions. Isotherm analysis (Figure S3 and Table 2) revealed a superior fit to the Langmuir model ($R^2 > 0.996$) compared to the Freundlich model, indicating that the adsorption of Pb(II) and Cd(II) on XBS occurs on a uniform surface, forming a monolayer on the adsorption sites. The maximum capacities (q_{max}) reached 224.72 mg/g for Pb(II) and 82.99 mg/g for Cd(II), closely matching the experimental values (q_{exp}), significantly exceeding unmodified white-rot fungus. The Freundlich parameters ($1/n < 1$ and high k_F values) confirmed favorable adsorption with strong chemisorption interactions between the functional groups of XBS and heavy metal ions, suggesting high affinity and effective binding.

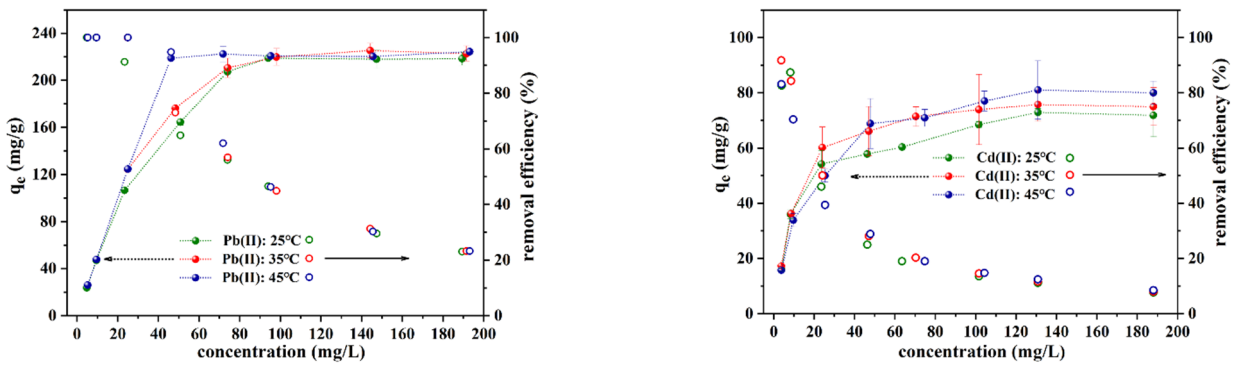


Figure 5. Effect of initial concentration on (**a**) Pb(II) and (**b**) Cd(II) adsorption by XBS at different temperatures. The solid arrow indicates removal efficiency, whereas the dotted arrow denotes q_e.

The magnitude of the heat of adsorption offers important insights into the nature of both the adsorbent surface and the adsorbed phase. To further explore the adsorption mechanism of Pb(II) and Cd(II) onto XBS, the thermodynamic parameters of adsorption, Gibbs free energy (ΔG), enthalpy (ΔH) and entropy (ΔS), were calculated and summarized in Table S1. Thermodynamic analysis yielded negative ΔG values (−5.500 to −11.931 kJ/mol for Pb(II), −1.265 to −1.863 kJ/mol for Cd(II)), confirming spontaneous adsorption. Positive ΔH values (89.647 kJ/mol for Pb(II), 7.697 kJ/mol for Cd(II)) revealed endothermic character, meaning that higher temperatures favor the adsorption process, as evidenced by the positive correlation between adsorption capacity and temperature. While positive ΔS (317.146 J/(mol/K) for Pb(II), 30.229 J/(mol/K) for Cd(II)) suggested increased interfacial disorder. The entropy-driven spontaneity, combined with minimal temperature dependence, positions XBS as a versatile adsorbent for practical wastewater treatment applications across diverse thermal conditions.

Table 2. Fitting parameters of Langmuir and Freundlich models for Pb(II) and Cd(II) adsorption by XBS.

Models	**Heavy Metal Ion**	**Pb(II)**			**Cd(II)**		
		298 K	**308 K**	**318 K**	**298 K**	**308 K**	**318 K**
	$q_{e,exp}$ (mg/g)	**218.88**	**225.30**	**224.30**	**72.90**	**75.70**	**80.98**
Langmuir	q_m (mg/g)	221.24	224.72	223.21	73.64	76.28	82.99
	k_L (L/min)	0.559	1.014	6.289	0.194	0.374	0.158
	R^2	0.999	0.999	1.000	0.996	0.999	0.998
Freundlich	k_F (mg/g)	99.13	144.38	218.20	25.67	28.35	21.46
	1/n	0.179	0.096	0.004	0.221	0.220	0.287
	R^2	0.910	0.813	0.456	0.834	0.912	0.951

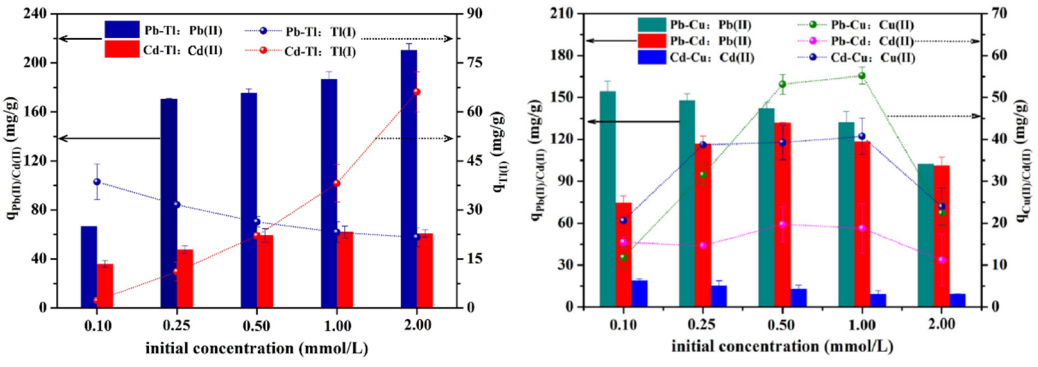
As shown in Table 3, XBS exhibits superior performance characteristics compared to conventional adsorbents across multiple critical parameters, due to its unique structural and chemical design. The material's exceptional performance is attributed to three key advantages: (1) The precursor materials of XBS are sustainably sourced from readily available fungal biomass. (2) Its preparation involves a single-step process that does not require thermal treatment, thereby reducing energy consumption and simplifying processing complexity. (3) The as-prepared XBS optimizes the pore architecture and incorporates special active functional groups. Despite this straightforward fabrication approach, XBS exhibits superior adsorption capacities for Pb(II) and Cd(II) compared to many reported biosorbents, including modified agricultural waste or fungal-derived materials. Furthermore, XBS enables rapid solid–liquid separation through gravity-driven settling or simple filtration, addressing a critical limitation of traditional biosorbents. These features collectively make XBS a promising candidate for wastewater treatment applications.

Table 3. Comparative analysis of adsorption performance of modified biomass-based adsorbents for Pb(II) or Cd(II).

Adsorbent	Preparation Method	Heavy Metal	pH	Time (min)	q_m (mg/g)	Suited Equilibrium Model Analysis	R^2 Values	Kinetics Model Analysis	R^2 Values	Reference
lignin-based porous carbon (LPC)	Mix lignin, urea, and ammonia water and stir evenly, then dry for 1 h. Heat and calcine for another 2 h. Finally, cool to room temperature.	Pb(II) Cd(II)	6.0	60	250.47 126.37	Freundlich	0.988 0.975	Pseudo-second-order	0.999 0.997	[38]
carnauba fruit biomass (CFB)	Wash the outer skin of the white wax fruit with distilled water, dry at 60 °C for 48 h, grind and sieve.	Pb(II) Cd(II)	5.0	120	27.74 34.16	Temkin Freundlich	0.981 0.993	Pseudo-second-order	1.000 1.000	[39]
tannin-immobilized cellulose fiber powder (TCF)	Mix NaOH, tannins, coconut shell cellulose, and epichlorohydrin in stages and heat to stir evenly for 6 h, then wash with water and dry at 40 °C for 24 h.	Pb(II) Cd(II)	5.0	30.00	38.02 59.52	Langmuir	0.997 0.993	-	-	[40]
rose damascena biomass power (RWB)	Heat Damascus rose powder at 120° C for 72 h, then treat with 0.2 M H_2SO_4 and NaOH separately, and finally dry at 105 °C.	Pb(II) Cd(II)	6.5	120	24.90 24.80	Langmuir	0.985 0.989	Pseudo-second-order	0.999 0.999	[41]
chemical treatment of corn stover powder	Treat corn stover with 0.1 M HNO_3 for 4 h, then wash with water, dry at 105° C, and grind.	Pb(II)	5.0	60	27.10	Langmuir	1.000	Pseudo-second-order	0.998	[42]
coffee husk biomass powder (CHBW)	After washing with water, the coffee shells are dried at 25 °C for one week and then ground into powder.	Pb(II)	5.0	60	19.02	Freundlich	0.980	Pseudo-second-order	1.000	[43]
sugarcane bagasse (SCB)	Boil the sugarcane bagasse in distilled water for 30 min, dry them in a hot air stove at 120 °C for 24 h, and finally grind them into powder.	Cd(II)	6.0	60	69.06	Langmuir	0.999	-	-	[44]
turbinaria ornate beads	Mix T. ornata and sodium alginate solution and stir at room temperature for 5 min. Add 2% $CaCl_2$ solution dropwise to the mixture to form microspheres, and finally immerse them in calcium chloride solution for 2 h before washing with water.	Cd(II)	6.8	90	23.90	Langmuir	0.998	Pseudo-second-order	0.990	[45]
XBS	Mix inactivated YK powder with NaOH and CS_2 for yellowing for 3 h, then freeze dry to form a macroporous sponge material.	Pb(II) Cd(II)	1 2	30 240	225.30 80.98	Langmuir	0.999 0.998	Pseudo-second-order	1.000 0.999	this study

3.2.4. Selective Adsorption Behaviors

To assess the impact of coexisting metal ions on adsorption selectivity, the adsorption behavior of XBS was investigated in several binary systems, including Pb-Tl, Pb-Cu, Pb-Cd, Cd-Tl, and Cd-Cu, which coexist in steel-making and copper-flotation copper-mining industries [46,47]. As illustrated in Figure 6, in Tl(I)-containing systems, XBS maintained excellent Pb(II) removal efficiency (>95%) with less than 5% capacity reduction, while Cd(II) adsorption decreased moderately (~15%) as Tl(I) concentration increased from 20.44 to 408.76 mg/L. The presence of Pb(II) has little effect on Tl(I) removal, with higher efficiency observed at lower concentrations. In contrast, the amount of Tl(I) adsorbed increases as Cd(II) concentrations rise, indicating a stronger affinity of XBS for Pb(II) over Tl(I) and Cd(II), likely due to differences in the physicochemical properties of the metal ions. Moreover, Cd(II) has an insignificant effect on Tl(I) removal, as the amount of Tl(I) adsorbed continues to increase, which is advantageous for the treatment of wastewater containing both metals. More pronounced competition was observed in Cu(II) systems, where Pb(II) and Cd(II) adsorption capacities decreased by 31% and 76%, respectively, with Cu(II) achieving a maximum adsorption of 55.32 mg/g (Pb-Cu system) and 40.75 mg/g (Cd-Cu system), indicating that XBS has a stronger affinity for Cu(II) than for Pb(II) or Cd(II). When Pb(II) coexists with Cd(II), the Pb(II) adsorption amount of XBS initially increases and then slightly decreases, while the Cd(II) adsorption remains within the range of 11 ~ 20 mg/g as concentrations increase. The co-existence of Pb(II) and Cd(II) reduces their respective removal efficiencies, with Pb(II) exerting a stronger inhibitory effect on Cd(II) removal than vice versa. According to the hard and soft acids and bases theory [48–50], the affinity of heavy metals for metal-binding donor atoms and ligands (such as S-, N-, and O-containing ligands) follows the order Cd(II) < Cu(II) < Pb(II) < Tl(I). The index X^2_{mr} (where X_m represents electronegativity and r represents ionic radius), which measures the importance of covalent interactions relative to ionic interactions [51], is as follows: 2.43 for Tl(I), 2.77 for Pb(II), 1.39 for Cu(II), and 1.64 for Cd(II). This suggests that ligands containing S, N, and O exhibit stronger binding preferences for Tl(I) and Pb(II) than for Cu(II) and Cd(II). Nevertheless, the higher Z^2/r value (Z representing formal charge), which reflects the magnitude of ionic energy for Pb(II) over Tl(I), confirms the superior removal capacity of XBS for Pb(II). Consequently, the adsorption selectivity of XBS for heavy metal ions follows the order: Pb(II) > Tl(I) > Cu(II) > Cd(II), which shows that XBS has a preferential selective adsorption for Pb(II).



(**a**) (**b**)

Figure 6. (**a**) Effect of Tl(I) on the competitive adsorption of Pb(II) and Cd(II) by XBS, The solid arrow indicates $q_{Pb(II)/Cd(II)}$, whereas the dotted arrow denotes $q_{Tl(II)}$. (**b**) Selective competitive adsorption of Pb(II), Cd(II) and Cu(II) by XBS, The solid arrow indicates $q_{Pb(II)/Cd(II)}$, whereas the dotted arrow denotes $q_{Cu(II)/Cd(II)}$.

The adsorption selectivity of XBS for heavy metal ions can be further rationalized by their distinct physicochemical properties (Table 4) [35,36]. Pb(II) demonstrates superior adsorption performance due to its combination of high electronegativity (2.33), strong binding affinity ($logK_{Scale, M}$ = 2.68), low hydrolysis tendency ($logK_{H2O, M}$ = −7.60) and favorable hydrated radius (4.01 Å). In contrast, Cd(II) exhibits the weakest adsorption affinity, attributed to its lower electronegativity (1.69), weaker binding strength (2.15), and larger hydrated radius (4.26 Å) that sterically hinders coordination. The intermediate adsorption capacities of Tl(I) (low binding strength at 0.46) and Cu(II) (high hydrolysis tendency at −7.50) further confirm the importance of these physicochemical properties in governing selectivity. These fundamental insights demonstrate how XBS's carefully designed functional groups, particularly the -C(=S)S- moieties, leverage both covalent and ionic interaction mechanisms to achieve exceptional Pb(II) selectivity while maintaining appreciable removal capacity for other heavy metals, making it highly effective for treating complex wastewater streams containing multiple metal contaminants.

Table 4. The physicochemical properties of four heavy metal ions.

Metal Ion Type	Ionic Radius	Pauling Electronegativity (PE)	Hydrated Radius (HR, Å)	Hardness Index (HI)	$logk_{Scale, M}$	$logk_{H2O, M}$
Pb(II)	1.19	2.33	4.01	0.131	2.68	−7.60
Cd(II)	0.97	1.69	4.26	0.081	2.15	−10.1
Tl(I)	1.50	1.62	3.30	0.106	0.46	−13.21
Cu(II)	0.73	1.90	4.19	0.104	2.66	−7.50

3.3. Reproducibility and Reusability Evaluations

The batch-to-batch consistency of XBS production was rigorously validated through several independent preparations under strictly controlled conditions. Standardized protocols were maintained throughout the entire preparation process, beginning with precise fungal cultivation (3 d on PDA medium at 30 ± 0.5 °C followed by 5 d in PDB culture) and extending through the optimized xanthation reaction (0.50 g YK, 37.5 mL 14 wt% NaOH, 2.0 mL CS_2, 3 h at 25 ± 0.5 °C). Quality assessments demonstrated exceptional reproducibility across multiple parameters: physical characteristics showed consistent color (light yellow) and texture (sponge-like); adsorption performance varied by less than 10% for Pb(II) and Cd(II), and kinetic performance remained highly consistent. Notably, normal environmental fluctuations during preparation had a negligible impact on product quality, confirming the robustness of the synthesis protocol. This demonstrated that reproducibility meets critical requirements for both reliable laboratory research and potential industrial scale-up. The consistent quality across multiple production batches underscores the reliability of XBS as a promising adsorbent for water treatment applications.

The regeneration performance of XBS was systematically investigated through three consecutive adsorption–desorption cycles, providing some insights for practical wastewater treatment applications (Figure 7). Both 0.5 M HNO_3 and HCl demonstrated effective desorption capabilities, with HNO_3 showing marginally superior efficiency (86% vs. 85% for Pb(II) and 85% vs. 84% for Cd(II)). However, subsequent adsorption cycles revealed progressive capacity decline, with Pb(II) retention decreasing to 58–60% after the first cycle and <26% by the third cycle, while Cd(II) performance dropped more severely to 28–41% initially and <10% ultimately. This performance degradation primarily stems from three mechanistic factors: (1) insufficient Na^+ replenishment due to omitted NaOH reactivation, impairing subsequent ion exchange capacity; (2) physical material loss occurred during washing procedures; and (3) irreversible damage to critical functional groups, especially the degradation of xanthate groups (S=C(R)-SNa) in the strong acidic conditions. These

findings highlight the need for optimized regeneration protocols incorporating alkaline reactivation steps, improved washing methodologies, and the potential chemical stabilization of functional groups.

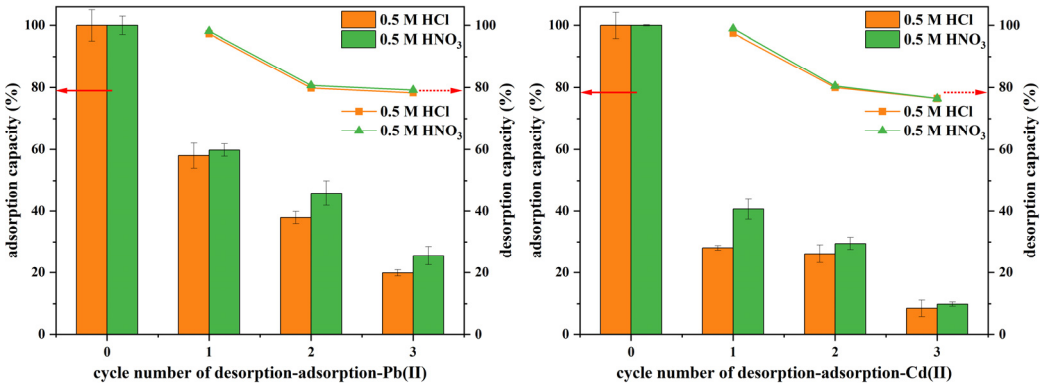


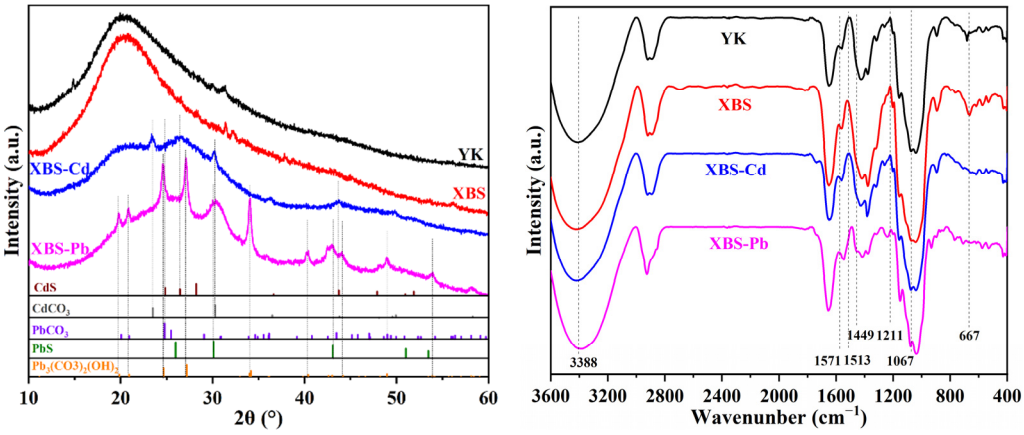
Figure 7. (**a**) Desorption and reusability efficiency of XBS for Pb(II); (**b**) desorption and reusability efficiency of XBS for Cd(II). The solid arrow indicates adsorption capacity, whereas the dotted arrow denotes desorption capacity.

3.4. Material Characterization and Adsorption Mechanism

XRD pattern analysis (Figure 8a) demonstrates significant structural transformations in XBS following metal adsorption. The broad peak at 20.47° in pristine XBS confirms its amorphous organic nature, while new crystalline phases emerge after Pb(II) and Cd(II) uptake. For Pb(II)-loaded XBS, distinct diffraction peaks at 30.10°, 43.08°, and 53.45°, corresponding to the (200), (220), and (222) crystal orientations of PbS (PDF#98-000-0223), and new peaks at 20.91°, 24.80°, and 49.39°, corresponding to the (020), (111), and (023) crystal planes of $PbCO_3$ (PDF#98-000-0153), are clearly observed after Pb(II) adsorption [52]. Additionally, characteristic diffraction peaks attributed to $Pb_3(CO_3)_2(OH)_2$ (PDF#98-000-0248) appear at 19.59° (101), 20.89° (012), 24.58° (104), 27.10° (015), 34.07° (009), 40.40° (202), and 53.90° (122) [53]. Similarly, newly formed peaks at 26.45°and 43.74°, corresponding to the (002) and (110) crystal planes of CdS (PDF#99-000-1412), as well as characteristic peaks at 23.52° (012) and 30.27° (104) associated with the hexagonal crystal structure of $CdCO_3$ (PDF#99-000-2764), are observed. These findings suggest that Pb(II) and Cd(II) ions might interact with active ligands, including S-containing groups, -OH and -COOH groups, leading to complexation and precipitation reactions on the surface of XBS [54]. These crystalline products, with their extremely low solubility products ($K_{sp}^{\theta}(PbS) = 1.3 \times 10^{-28}$, $K_{sp}^{\theta}(CdS) = 8.0 \times 10^{-27}$, $K_{sp}^{\theta}(PbCO_3) = 7.4 \times 10^{-14}$, $K_{sp}^{\theta}(CdCO_3) = 5.2 \times 10^{-12}$ and $K_{sp}^{\theta}(Pb(OH)_2) = 1.2 \times 10^{-15}$) [55,56], confirm the predominance of precipitation mechanisms alongside surface complexation. Consequently, the primary mechanism for the removal of Pb(II) and Cd(II) by XBS is similar.

FTIR spectroscopy confirmed the structural evolution of XBS after xanthate modification and metal adsorption (Figure 8b). Compared to the original YK fungus, XBS exhibited enhanced absorption intensities at 1571 cm^{-1}, 1513–1211 cm^{-1} and 1067–667 cm^{-1}, indicating that the xanthate modification had a significant effect on the structure of the material. Key spectral features included characteristic peaks at 3388 cm^{-1} (-OH/-NH_2 stretching) and 1449 cm^{-1} (N-H bending), which showed significant shifts after metal adsorption, indicating coordination through -NH_2/N-H groups [57–59]. The characteristic absorption peaks at 1067 cm^{-1} attributed to -O-C(=S)-S and 1211 cm^{-1} corresponding to C-O groups exhibited marked intensity changes, further confirming their participation in Pb(II)/Cd(II) chemisorption [60,61], while the distinct C-S peak at 667 cm^{-1} verified successful xanthate

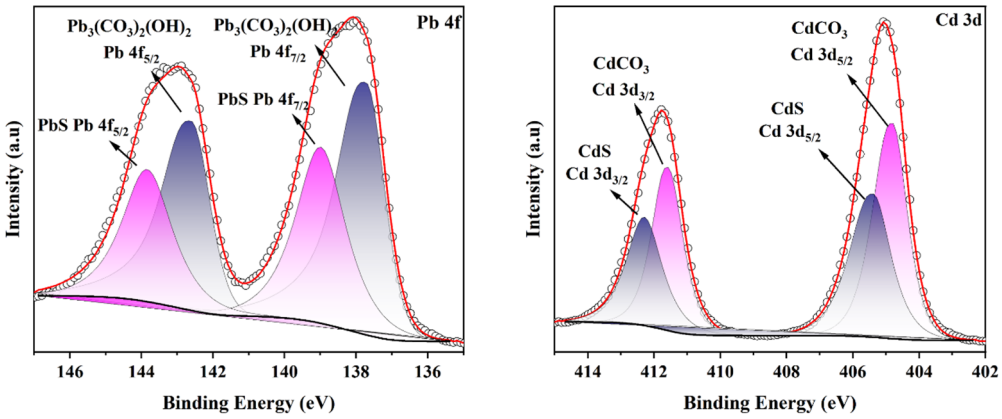
incorporation [62]. Notably, Pb(II) induced more pronounced spectral changes than Cd(II), correlating with XBS's superior affinity for Pb(II). These results demonstrate that heavy metal adsorption occurs primarily through chemical complexation with S/N/O-containing functional groups, with xanthate moieties playing a pivotal role.



(**a**) (**b**)

Figure 8. XRD (**a**) and FTIR (**b**) spectra of YK, XBS before and after adsorption.

The XPS analysis (Figure S4 and Figure 9) provides further evidence for the adsorption mechanism of Pb(II) and Cd(II) on XBS. The survey spectra confirm the presence of S, C, N, O, and Na as the primary elements in XBS, with new peaks emerging at 138.94 eV (Pb 4f) and 405.46 eV (Cd 3d) after adsorption. The observed redshift and weakening of the Na 1s peak indicate ion exchange between Na^+ and Pb(II)/Cd(II) ions, facilitating the complexation of Pb(II)/Cd(II) with the xanthate groups (S=C(R)-SNa) [63]. High-resolution spectra of Pb 4f reveal two symmetrical peaks at 142.61 eV and 143.84 eV, while Cd 3d exhibits peaks at 405.39 eV and 412.3 eV, suggesting the formation of hydroxide, acetate, and/or sulfide species on the XBS surface [64]. These findings align with the XRD results, confirming the coexistence of multiple adsorption mechanisms.



(**a**) (**b**)

Figure 9. Pb 4f (**a**) and Cd 3d (**b**) core-level deconvoluted spectra of XBS after Pb(II) and Cd(II) adsorption.

High-resolution XPS spectra (Figure 10) reveal the critical role of functional groups in Pb(II)/Cd(II) adsorption on XBS. The C 1s spectrum (Figure 10a) shows four characteristic peaks at 284.80 eV (C-H/C=C), 286.37 eV (C-O-C/C-OH), 287.80 eV (C=O), and 289.71 eV (HO-C=O), with xanthation altering electronic distributions and weakening adjacent C-C bonds [63,65,66]. Post-adsorption changes in -COOH and -OH peak intensities

and areas confirm their participation in metal complexation [67]. In the N 1s spectrum (Figure 10b), the strength of the nitrogen-containing group was greatly reduced before and after modification, due to the destruction of the nitrogen-containing group by the xanthan acidification reaction [65]. The N 1s spectrum displays three nitrogen states (398.53 eV for -N=C, 399.62 eV for -NH_2 and 400.64 eV for -N-C-), where Pb(II) induces a significant -NH_2 shift to 400.34 eV indicating strong chelation [68,69]. The binding energies (BEs) of the -N-C- and -N=C groups also undergo significant shifts after adsorption, likely due to chelation between the amine groups and Pb(II), which affects the charge distribution state of the -N-C- and -N=C groups [53]. Additionally, following the adsorption of Cd(II), the BE of the -N=C group shifted to 399.21 eV, possibly due to electrostatic interactions and ion exchange [70]. In the O 1s spectrum (Figure 10c), the slight increase in the content of -OH groups before and after modification suggests the presence of residual -OH groups during xanthan modification. The peaks of XBS at 533.85 eV (O-C), 532.81 eV (C=O), 531.44 eV (O-H) and 534.0 eV (adsorbed water) indicate an increase in the C=O/O-C=O content, implying that the adsorption process consumes a significant amount of -COOH. Following the adsorption of Pb(II) and Cd(II), the O1s peak shifted towards higher binding energies. These outcomes suggest that complex reactions occur between functional groups, such as -COOH and -OH, and Pb(II)/Cd(II) [71,72]. This further supports the presence of Pb(II) and Cd(II) on XBS in the forms of hydroxides or acetates. Most notably, the S 2p spectrum (Figure 10d) confirms successful xanthation through S-Na (161.59 eV), C-S (163.57 eV), and S-O (167.95 eV) peaks. After the adsorption of Pb(II)/Cd(II), the S-Na binding band is transformed into S-Pb/S-Cd bonds, indicating an ion-exchange interaction. The BEs of the sulfur oxide compounds change following the adsorption of Pb(II) and Cd(II), suggesting that the sulfur heteroatoms within the S-H and S=O groups coordinate with these metals [73]. These results collectively demonstrate that XBS achieves superior heavy metal removal through the synergistic effects of xanthate-enabled ion exchange, multi-dentate complexation via S/N/O functional groups, and chemical precipitation.

Therefore, XBS achieves highly efficient and stable immobilization of Pb(II) and Cd(II) through a synergistic combination of three complementary mechanisms (Figure 11). The removal process initiates with electrostatic attraction, where the negatively charged XBS surface rapidly captures cationic Pb(II) and Cd(II) species, accompanied by ion exchange with surface Na(I) ions. Subsequently, complexation dominates as Pb(II) preferentially coordinates with various functional groups (-O-C(=S)-S-, -OH, -COO- and -NH_2), forming stable surface complexes, while Cd(II) undergoes analogous but weaker binding. The final immobilization stage involves in situ precipitation, where residual alkalinity from synthesis triggers xanthate hydrolysis, resulting in the formation of highly insoluble PbS, $Pb_3(CO_3)_3(OH)_2$, CdS, and $CdCO_3$ precipitates. This hierarchical removal process, combining rapid initial capture (electrostatic), strong intermediate retention (complexation), and permanent final stabilization (precipitation), ensures robust heavy metal fixation. The multiple coordination pathways from other active functional groups provide redundant binding sites that collectively contribute to XBS's exceptional adsorption capacity and selectivity.

3.5. Economic Assessment

Beyond its adsorption capabilities, the practical implementation of XBS necessitates consideration of various economic factors. To address this, an economic evaluation was conducted. The adsorbent's room-temperature synthesis eliminates energy-intensive thermal processing, reducing production energy requirements compared to conventional adsorbents like activated carbon. Furthermore, XBS's inherent three-dimensional porous structure enables efficient solid–liquid separation post-adsorption, further lowering separation costs.

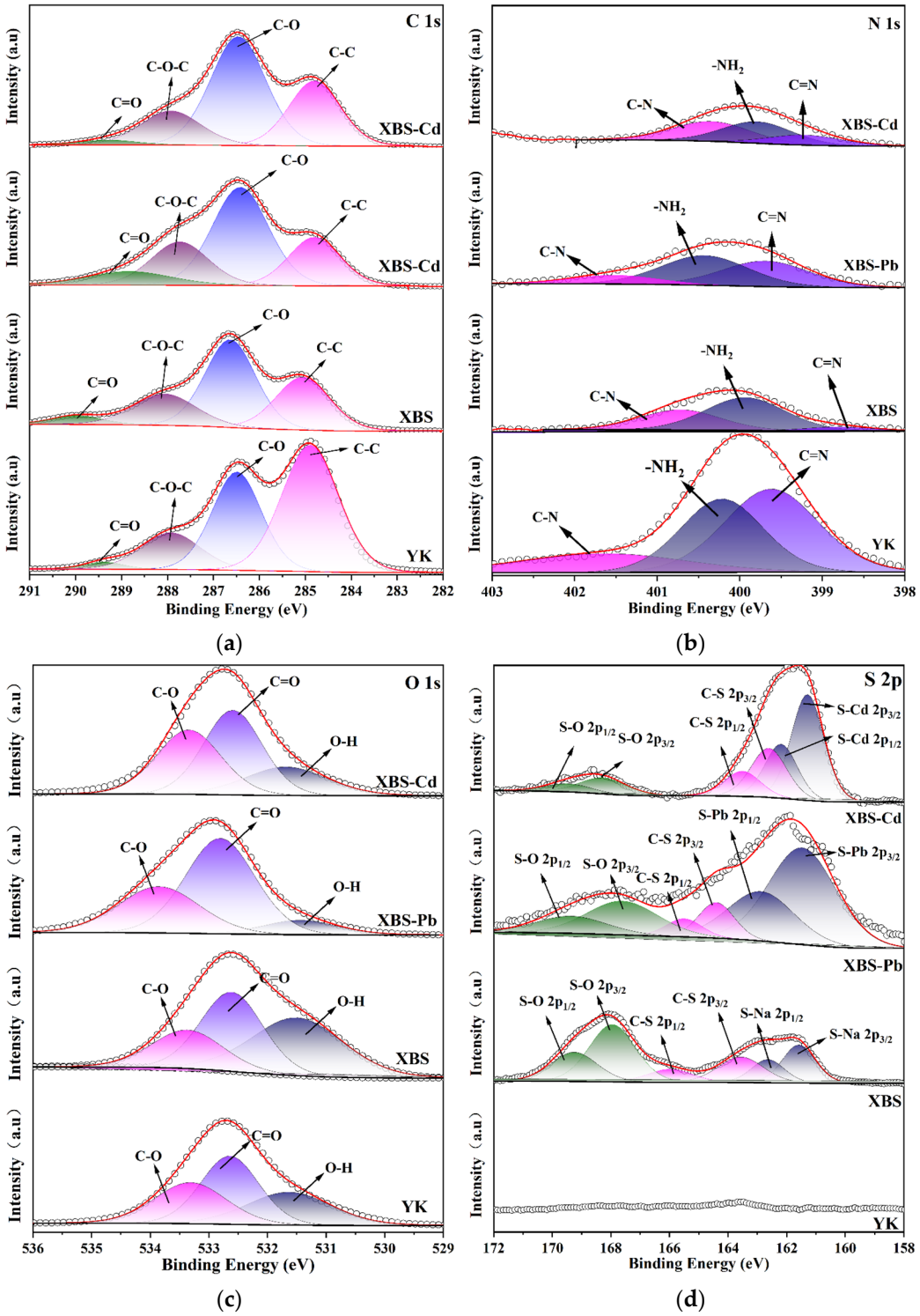


Figure 10. Signal regions of C 1s (**a**), N 1s (**b**), O 1s (**c**) and S 2p (**d**) for YK, XBS before and after Pb(II) and Cd(II) adsorption.

Based on available data, the economic assessment accounts for the consumption of chemicals and energy to deliver a comprehensive cost analysis. The estimated cost per batch of experiments is approximately USD 19.77. Considering the quantity of material synthesized per batch, it can effectively treat approximately 2700 L of target contaminant-containing wastewater, resulting in a cost of roughly USD 4.41 per ton of wastewater. Table 5 provides specific estimated values supporting this analysis. This economic evaluation demonstrates that XBS exhibits exceptional adsorption performance and offers significant

economic advantages over traditional wastewater treatment methods. Its cost-effectiveness, combined with these favorable operational characteristics, enhances the feasibility and practical implementation potential of XBS in real-world applications.

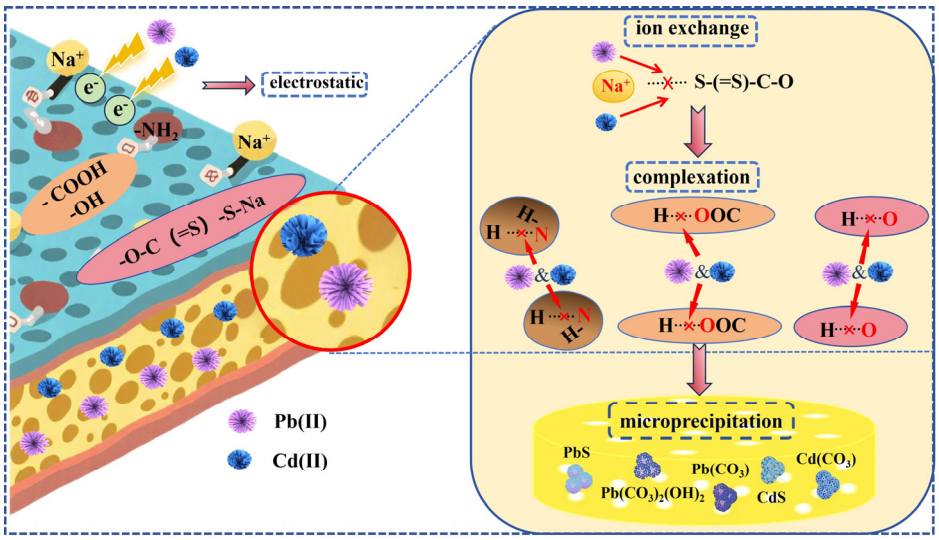


Figure 11. Mechanism diagram of Pb(II) and Cd(II) adsorption on XBS.

Table 5. Experimental inputs and energy consumption from one batch (one batch for 1 kg XBS).

Materials	Flow per Batch	Cost/USD per Ton Market Price in China (June 2025)	Cost/USD per Batch
Water for adsorbents preparation (L)	50	0.59	0.03
Water for adsorption (L)	500	0.59	0.30
White-rot fungi YK-624 contains culture medium (kg)	5	2100	10.50
NaOH (kg)	6.1	471	2.87
CS_2 (L)	2	694	1.77
Electricity		0.15/kWh	
Mixing (kWh)	3.6	0.15	0.54
Washing(kWh)	3	0.15	0.46
Drying	2	0.15	0.30
Adsorption (kWh)	20	0.15	3.00
Total			19.77

4. Conclusions

The development of xanthate-modified fungal adsorbent (XBS) represents a significant advancement in heavy metal remediation technology. Unlike conventional adsorbents, XBS exhibits exceptional adsorption capabilities, achieving removal efficiencies of 99% (11.88 mg/L) for Pb(II) and 40% (11.88 mg/L) for Cd(II) within just 5 min, with maximum capacities of 224.72 mg/g for Pb(II) and 82.99 mg/g for Cd(II). Its unique 3D porous structure enables rapid kinetics while facilitating easy separation, addressing key limitations of conventional adsorbents. The material exhibits superior selectivity (Pb(II) > Tl(I) > Cu(II) > Cd(II)) in complex systems. The material's superior performance stems from synergistic mechanisms: an initial ion exchange facilitates metal capture, followed by complexation with sulfur-, nitrogen-, and oxygen-containing functional groups, culminating in precipitation as stable mineral phases (metal sulfides and carbonates) that ensure permanent immobilization. Particularly noteworthy is XBS's inherent selectivity for Pb(II), which persists even in complex multi-metal systems. This is a critical advantage for real wastewater treatment scenarios. From an engineering perspective, the simplicity of XBS's

one-pot synthesis using fungal biomass presents distinct advantages in scalability and cost-effectiveness compared to synthetic alternatives. The material's inherent Pb(II) selectivity specifically targets priority contaminants in mining and electroplating wastewater. Combined with its biological origin, these features establish XBS as an environmentally sustainable solution that outperforms conventional treatment methods. Moving forward, research should focus on optimizing dynamic flow systems and developing regeneration protocols to facilitate commercial implementation. This work not only establishes XBS as a high-performance solution for heavy metal removal but also validates fungal-derived materials as a versatile platform for water treatment, bridging the gap between biological sustainability and engineered functionality for environmental applications.

Supplementary Materials: The following supporting information can be downloaded at: https://www.mdpi.com/article/10.3390/separations12070172/s1, Text S1 Data analysis: Adsorption kinetics [73,74]; Figure S1: N_2 adsorption/desorption isotherms of XBS; Figure S2: Plots of pseudo first-order and pseudo second-order kinetic equations of Pb(II) (a, b) and Cd(II) (c, d) adsorption by XBS; Figure S3: Langmuir and Freundlich fitting plots of Pb(II) (a, c) and Cd(II) (b, d) adsorption under different temperatures; Figure S4: XPS full spectra of YK, XBS before and after adsorption of Pb(II) and Cd(II); Table S1: The thermodynamic parameters for Pb(II) adsorption by XBS over the temperature ranges from 298 to 318 K.

Author Contributions: Conceptualization, N.W.; methodology, R.H. and Y.C.; software, C.W., Z.C. and Z.L.; validation, H.C., Z.L. and M.F.; formal analysis, C.W., Z.C., H.N. and R.H.; investigation, R.H., Y.C., H.N., H.C. and M.F.; resources, N.W. and J.W.; data curation, Z.L., M.F., H.C. and Y.C.; writing—original draft preparation, C.W., Z.C. and M.C.; writing—review and editing, N.W. and J.W.; visualization, M.C.; supervision, N.W. and M.C.; project administration, N.W.; funding acquisition, N.W. and M.C. All authors have read and agreed to the published version of the manuscript.

Funding: This research was funded by the National Natural Science Foundation of China (42277202), the Postdoctoral Scientific Research Program of Guangzhou (No. 624021-58), and the China Postdoctoral Science Foundation (No. 2024M760623).

Data Availability Statement: Data will be made available on request.

Acknowledgments: The authors gratefully acknowledge the fund support from the National Natural Science Foundation of China (42277202), the Postdoctoral Scientific Research Program of Guangzhou (No. 624021-58) and the China Postdoctoral Science Foundation (No. 2024M760623).

Conflicts of Interest: The authors declare no conflicts of interest.

References

1. Han, X.; Li, P.; Zhang, M.; Wang, J.; Cao, Y.; Zhang, T.; Zhou, G.; Li, F. Designing three-dimensional half-embedded ES-PAN/AHCNs adsorption membrane for removal of Pb(II), Cu(II) and Cr(III). *Colloids Surf. A Physicochem. Eng. Aspects* **2021**, *627*, 127177. [CrossRef]
2. Sun, J.; Hu, R.; Zhao, X.; Liu, T.; Bai, Z. A novel chitosan/cellulose phosphonate composite hydrogel for ultrafast and efficient removal of Pb(II) and Cu(II) from wastewater. *Carbohydr. Polym.* **2024**, *336*, 122104. [CrossRef] [PubMed]
3. Zhang, L.; Zhu, Y.; Gu, H.; Lam, S.S.; Chen, X.; Sonne, C.; Peng, W. A review of phytoremediation of environmental lead (pb) contamination. *Chemosphere* **2024**, *362*, 142691. [CrossRef] [PubMed]
4. Yang, Y.; Zhang, Y.; Zheng, H.; Zhang, B.; Zuo, Q.; Fan, K. Functionalized dual modification of covalent organic framework for efficient and rapid trace heavy metals removal from drinking water. *Chemosphere* **2022**, *290*, 133215. [CrossRef]
5. Rashmi, N.; Salmataj, S.A.; Kumar, P.S.; Bhat, P. Exploring chemically and physically modified plant-based fiber biomass for biosorption in wastewater treatment: A concise review. *J. Water Process Eng.* **2024**, *67*, 106245. [CrossRef]
6. Wu, J.; Cheng, X.; Li, Y.; Yang, G. Constructing biodegradable nanochitin-contained chitosan hydrogel beads for fast and efficient removal of Cu(II) from aqueous solution. *Carbohydr. Polym.* **2019**, *211*, 152–160. [CrossRef]
7. Oladoye, P.O. Natural, low-cost adsorbents for toxic Pb(II) ion sequestration from (waste)water: A state-of-the-art review. *Chemosphere* **2022**, *287*, 132130. [CrossRef]

8. Modwi, A.; Elamin, N.Y.; Al-Ayed, A.S.; Ismail, M.; Taha, K.K. Pb(II) ions removal via green spinel $NiFe_2O_4$ loaded on g-C_3N_4 nanomaterials. *Nano-Struct. Nano-Objects* **2023**, *35*, 101031. [CrossRef]
9. Amarray, A.; El Ghachtouli, S.; Leroy, J.; Bonnaillie, P.; Khaless, K.; Dahbi, M.; Azzi, M. Mesoporous nanomaterials based on manganese with different interlayer alkali cations: An efficient approach for the removal of Pb(II) and Cd(II) from aqueous medium. *J. Water Process Eng.* **2021**, *40*, 101944. [CrossRef]
10. Bilal, M.; Ihsanullah, I.; Younas, M.; Ul Hassan Shah, M. Recent advances in applications of low-cost adsorbents for the removal of heavy metals from water: A critical review. *Sep. Purif. Technol.* **2021**, *278*, 119510. [CrossRef]
11. Yin, W.; Dai, D.; Hou, J.; Wang, S.; Wu, X.; Wang, X. Hierarchical porous biochar-based functional materials derived from biowaste for Pb(II) removal. *Appl. Surf. Sci.* **2019**, *465*, 297–302. [CrossRef]
12. Shooto, N.D. Removal of toxic hexavalent chromium (Cr(VI)) and divalent lead (Pb(II)) ions from aqueous solution by modified rhizomes of Acorus calamus. *Surf. Interfaces* **2020**, *20*, 100624. [CrossRef]
13. Bangaraiah, P.; Peele, K.A.; Venkateswarulu, T.C. Removal of lead from aqueous solution using chemically modified green algae as biosorbent: Optimization and kinetics study. *Int. J. Environ. Sci. Technol.* **2020**, *18*, 317–326. [CrossRef]
14. Huang, F.; Gao, L.-Y.; Wu, R.-R.; Wang, H.; Xiao, R.-B. Qualitative and quantitative characterization of adsorption mechanisms for Cd^{2+} by silicon-rich biochar. *Sci. Total Environ.* **2020**, *731*, 139163. [CrossRef] [PubMed]
15. Palabıyık, B.B.; Selcuk, H.; Oktem, Y.A. Cadmium removal using potato peels as adsorbent: Kinetic studies. *Desalin. Water Treat.* **2019**, *172*, 148–157. [CrossRef]
16. Zhang, D.; Yin, C.P.; Abbas, N.; Mao, Z.C.; Zhang, Y.L. Multiple heavy metal tolerance and removal by an earthworm gut fungus *Trichoderma brevicompactum* QYCD-6. *Sci. Rep.* **2020**, *10*, 6940. [CrossRef] [PubMed]
17. Yu, C.; Wang, X.; Huang, S.; Zhang, X.; An, X.; Xu, M.; Lian, B. Characterisation of products from fungally modified wollastonite and the simulation experiment of Pb^{2+} fixation. *Sci. Total Environ.* **2021**, *760*, 143357. [CrossRef]
18. Li, Y.; Zou, G.; Yang, S.; Wang, Z.; Chen, T.; Yu, X.; Guo, Q.; He, R.; Duan, T.; Zhu, W. Integration of bio-inspired adsorption and photodegradation for the treatment of organics-containing radioactive wastewater. *Chem. Eng. J.* **2019**, *364*, 139–145. [CrossRef]
19. Enayatizamir, N.; Liu, J.; Wang, L.; Lin, X.; Fu, P. Coupling Laccase production from Trametes pubescence with heavy metal removal for Economic Waste Water Treatment. *J. Water Process Eng.* **2020**, *37*, 101357. [CrossRef]
20. Sharma, K.R.; Giri, R.; Sharma, R.K. Lead, cadmium and nickel removal efficiency of white-rot fungus *Phlebia brevispora*. *Lett. Appl. Microbiol.* **2020**, *71*, 637–644. [CrossRef]
21. Ma, X.; Li, X.; Liu, J.; Cheng, Y.; Zhai, F.; Sun, Z.; Han, L. Enhancing *Salix viminalis* L.-mediated phytoremediation of polycyclic aromatic hydrocarbon-contaminated soil by inoculation with *Crucibulum laeve* (white-rot fungus). *Environ. Sci. Pollut. Res.* **2020**, *27*, 41326–41341. [CrossRef] [PubMed]
22. Chen, L.; Zhang, X.; Zhang, M.; Zhu, Y.; Zhuo, R. Removal of heavy-metal pollutants by white rot fungi: Mechanisms, achievements, and perspectives. *J. Clean. Prod.* **2022**, *354*, 131681. [CrossRef]
23. Priya, A.K.; Gnanasekaran, L.; Dutta, K.; Rajendran, S.; Balakrishnan, D.; Soto-Moscoso, M. Biosorption of heavy metals by microorganisms: Evaluation of different underlying mechanisms. *Chemosphere* **2022**, *307*, 135957. [CrossRef] [PubMed]
24. Zhou, B.; Zhang, T.; Wang, F. Microbial-Based Heavy Metal Bioremediation: Toxicity and Eco-Friendly Approaches to Heavy Metal Decontamination. *Appl. Sci.* **2023**, *13*, 8439. [CrossRef]
25. Fan, M.Q.; Wang, X.; Song, Q.; Zhang, L.Y.; Ren, B.; Yang, X.D. Review of biomass-based materials for uranium adsorption. *J. Radioanal. Nucl. Chem.* **2021**, *330*, 589–602. [CrossRef]
26. Lu, N.; Hu, T.; Zhai, Y.; Qin, H.; Aliyeva, J.; Zhang, H. Fungal cell with artificial metal container for heavy metals biosorption: Equilibrium, kinetics study and mechanisms analysis. *Environ. Res.* **2020**, *182*, 109061. [CrossRef]
27. Kordialik-Bogacka, E.; Diowksz, A. Metal uptake capacity of modified Saccharomyces pastorianus biomass from different types of solution. *Environ. Sci. Pollut. Res.* **2013**, *21*, 2223–2229. [CrossRef]
28. Wang, N.N.; Xu, X.J.; Li, H.Y.; Yuan, L.Z.; Yu, H.W. Enhanced Selective Adsorption of Pb(II) from Aqueous Solutions by One-Pot Synthesis of Xanthate-Modified Chitosan Sponge: Behaviors and Mechanisms. *Ind. Eng. Chem. Res.* **2016**, *55*, 12222–12231. [CrossRef]
29. Nieboer, E.; Richardson, D.H.S. The replacement of the nondescript term 'heavy metals' by a biologically and chemically significant classification of metal ions. *Environ. Pollut. Ser. B Chem. Phys.* **1980**, *1*, 3–26. [CrossRef]
30. Lin, C.; Dong, B.; Xu, Z. Competitive adsorption of heavy metals onto xanthate-modified sludge hydrochar and its solidification as secondary minerals. *Chemosphere* **2024**, *356*, 141878. [CrossRef]
31. Wang, N.; Qiu, Y.; Hu, K.; Huang, C.; Xiang, J.; Li, H.; Tang, J.; Wang, J.; Xiao, T. One-step synthesis of cake-like biosorbents from plant biomass for the effective removal and recovery heavy metals: Effect of plant species and roles of xanthation. *Chemosphere* **2021**, *266*, 129129. [CrossRef] [PubMed]
32. Drumm, F.C.; Grassi, P.; Georgin, J.; Tonato, D.; Pfingsten Franco, D.S.; Chaves Neto, J.R.; Mazutti, M.A.; Jahn, S.L.; Dotto, G.L. Potentiality of the *Phoma* sp. inactive fungal biomass, a waste from the bioherbicide production, for the treatment of colored effluents. *Chemosphere* **2019**, *235*, 596–605. [CrossRef] [PubMed]

33. Khambhaty, Y.; Mody, K.; Basha, S.; Jha, B. Kinetics, equilibrium and thermodynamic studies on biosorption of hexavalent chromium by dead fungal biomass of marine Aspergillus niger. *Chem. Eng. J.* **2009**, *145*, 489–495. [CrossRef]
34. Mercier, L.; Pinnavaia, T.J. Access in mesoporous materials: Advantages of a uniform pore structure in the design of a heavy metal ion adsorbent for environmental remediation. *Adv. Mater.* **1997**, *9*, 500–503. [CrossRef]
35. Benettayeb, A.; Guibal, E.; Morsli, A.; Kessas, R. Chemical modification of alginate for enhanced sorption of Cd(II), Cu(II) and Pb(II). *Chem. Eng. J.* **2017**, *316*, 704–714. [CrossRef]
36. Kinraide, T.B.; Yermiyahu, U. A scale of metal ion binding strengths correlating with ionic charge, Pauling electronegativity, toxicity, and other physiological effects. *J. Inorg. Biochem.* **2007**, *101*, 1201–1213. [CrossRef]
37. Sutherland, C. A method of classifying the influence of intraparticle diffusion in adsorption systems: Characteristic curves of the diffusion-chemisorption kinetic model. *Environ. Toxicol. Chem.* **2025**, *44*, 1209–1221. [CrossRef]
38. Wang, A.; Zheng, Z.; Li, R.; Hu, D.; Lu, Y.; Luo, H.; Yan, K. Biomass-derived porous carbon highly efficient for removal of Pb(II) and Cd(II). *Green Energy Environ.* **2019**, *4*, 414–423. [CrossRef]
39. Oliveira, M.R.F.; do Vale Abreu, K.; Romao, A.L.E.; Davi, D.M.B.; de Carvalho Magalhaes, C.E.; Carrilho, E.N.V.M.; Alves, C.R. Carnauba (*Copernicia prunifera*) palm tree biomass as adsorbent for Pb(II) and Cd(II) from water medium. *Environ. Sci. Pollut. Res.* **2021**, *28*, 18941–18952. [CrossRef]
40. Taksitta, K.; Sujarit, P.; Ratanawimarnwong, N.; Donpudsa, S.; Songsrirote, K. Development of tannin-immobilized cellulose fiber extracted from coconut husk and the application as a biosorbent to remove heavy metal ions. *Environ. Nanotechnol. Monit. Manag.* **2020**, *14*, 100389. [CrossRef]
41. Batool, F.; Mohyuddin, A.; Amjad, A.; ul Hassan, A.; Nadeem, S.; Javed, M.; Hafiz Dzarfan Othman, M.; Wayne Chew, K.; Rauf, A.; Kurniawan, T.A. Removal of Cd(II) and Pb(II) from synthetic wastewater using Rosa damascena waste as a biosorbent: An insight into adsorption mechanisms, kinetics, and thermodynamic studies. *Chem. Eng. Sci.* **2023**, *280*, 119072. [CrossRef]
42. Guyo, U.; Mhonyera, J.; Moyo, M. Pb(II) adsorption from aqueous solutions by raw and treated biomass of maize stover—A comparative study. *Process Saf. Environ. Prot.* **2015**, *93*, 192–200. [CrossRef]
43. Alhogbi, B.G. Potential of coffee husk biomass waste for the adsorption of Pb(II) ion from aqueous solutions. *Sustain. Chem. Pharm.* **2017**, *6*, 21–25. [CrossRef]
44. Garg, U.; Kaur, M.P.; Jawa, G.K.; Sud, D.; Garg, V.K. Removal of cadmium(II) from aqueous solutions by adsorption on agricultural waste biomass. *J. Hazard. Mater.* **2008**, *154*, 1149–1157. [CrossRef]
45. Fawzy, M.A.; Darwish, H.; Alharthi, S.; Al-Zaban, M.I.; Noureldeen, A.; Hassan, S.H.A. Process optimization and modeling of Cd^{2+} biosorption onto the free and immobilized *Turbinaria ornata* using Box–Behnken experimental design. *Sci. Rep.* **2022**, *12*, 3256. [CrossRef]
46. Liu, J.; Ren, S.; Zhou, Y.; Tsang, D.C.W.; Lippold, H.; Wang, J.; Yin, M.; Xiao, T.; Luo, X.; Chen, Y. High contamination risks of thallium and associated metal(loid)s in fluvial sediments from a steel-making area and implications for environmental management. *J. Environ. Manag.* **2019**, *250*, 109513. [CrossRef] [PubMed]
47. Mikoda, B.; Gruszecka-Kosowska, A. Mineral and chemical characteristics, textural parameters, and the mobility of the selected elements of flotation waste, originating from the Polish copper- mining industry. *Hum. Ecol. Risk Assess.* **2018**, *24*, 1216–1232. [CrossRef]
48. Bulin, C.; Zheng, R.; Guo, T.; Zhang, B. Incorporating hard-soft acid-base theory in multi-aspect analysis of the adsorption mechanism of aqueous heavy metals by graphene oxide. *J. Phys. Chem. Solids* **2022**, *170*, 110934. [CrossRef]
49. Pearson, R.G. Hard and Soft Acids and Bases. *J. Am. Chem. Soc.* **1963**, *85*, 3533–3539. [CrossRef]
50. Xia, Y.; Liao, G.; Wang, Z.; Wei, Y.; Liu, H.; Tang, Y.; Tang, H.; Liu, X.; Shi, J.; Liu, C. Efficient and deep adsorption of thallium(I) from complex water based on hard-soft acid-base theory. *Sep. Purif. Technol.* **2025**, *360*, 131221. [CrossRef]
51. Meng, X.; Wang, X.; Ma, Y.; Wang, Y. Development of a coupled model of quantitative ion character-activity relationships-biotic ligand model (QICARs-BLM) for predicting toxicity for data poor metals. *J. Hazard. Mater.* **2019**, *373*, 620–629. [CrossRef]
52. Zhou, S.; Huo, X.; Hua, M.; Luo, G.; Fan, J.; Clark, J.H.; Zhang, S. Insights on the Effect of Heavy Metals on Subcritical Hydrothermal Recycling of Heavy Metal-Contaminated Biomass and Its Derived Porous Carbon Properties Using Cu as a Case. *ACS ES&T Eng.* **2022**, *2*, 2245–2253. [CrossRef]
53. Haris, M.; Usman, M.; Su, F.; Lei, W.; Saleem, A.; Hamid, Y.; Guo, J.; Li, Y. Programmable synthesis of exfoliated biochar nanosheets for selective and highly efficient adsorption of thallium. *Chem. Eng. J.* **2022**, *434*, 134842. [CrossRef]
54. Cao, Y.; Xiao, W.; Shen, G.; Ji, G.; Zhang, Y.; Gao, C.; Han, L. Carbonization and ball milling on the enhancement of Pb(II) adsorption by wheat straw: Competitive effects of ion exchange and precipitation. *Bioresour. Technol.* **2019**, *273*, 70–76. [CrossRef] [PubMed]
55. Chen, H.; Min, F.; Hu, X.; Ma, D.; Huo, Z. Biochar assists phosphate solubilizing bacteria to resist combined Pb and Cd stress by promoting acid secretion and extracellular electron transfer. *J. Hazard. Mater.* **2023**, *452*, 131176. [CrossRef] [PubMed]

56. Zhang, X.; Zeng, L.; Wang, Y.; Tian, J.; Wang, J.; Sun, W.; Han, H.; Yang, Y. Selective separation of metals from wastewater using sulfide precipitation: A critical review in agents, operational factors and particle aggregation. *J. Environ. Manag.* **2023**, *344*, 118462. [CrossRef]
57. Branca, C.; D'Angelo, G.; Crupi, C.; Khouzami, K.; Rifici, S.; Ruello, G.; Wanderlingh, U. Role of the OH and NH vibrational groups in polysaccharide-nanocomposite interactions: A FTIR-ATR study on chitosan and chitosan/clay films. *Polymer* **2016**, *99*, 614–622. [CrossRef]
58. Chen, X.; Jiang, S.; Wu, J.; Yi, X.; Dai, G.; Shu, Y. Three-year field experiments revealed the immobilization effect of natural aging biochar on typical heavy metals (Pb, Cu, Cd). *Sci. Total Environ.* **2024**, *912*, 169384. [CrossRef]
59. Zhu, Y.; Hu, J.; Wang, J. Competitive adsorption of Pb(II), Cu(II) and Zn(II) onto xanthate-modified magnetic chitosan. *J. Hazard. Mater.* **2012**, *221–222*, 155–161. [CrossRef]
60. Chen, M.; Wang, X.; Zhang, H. Comparative research on selective adsorption of Pb(II) by biosorbents prepared by two kinds of modifying waste biomass: Highly-efficient performance, application and mechanism. *J. Environ. Manag.* **2021**, *288*, 112388. [CrossRef]
61. Singha, A.S.; Guleria, A. Chemical modification of cellulosic biopolymer and its use in removal of heavy metal ions from wastewater. *Int. J. Biol. Macromol.* **2014**, *67*, 409–417. [CrossRef]
62. Córdova, B.M.; Infantas, G.C.; Mayta, S.; Huamani-Palomino, R.G.; Kock, F.V.C.; Montes de Oca, J.; Valderrama, A.C. Xanthate-modified alginates for the removal of Pb(II) and Ni(II) from aqueous solutions: A brief analysis of alginate xanthation. *Int. J. Biol. Macromol.* **2021**, *179*, 557–566. [CrossRef] [PubMed]
63. Herath, A.; Layne, C.A.; Perez, F.; Hassan, E.I.B.; Pittman, C.U.; Mlsna, T.E. KOH-activated high surface area Douglas Fir biochar for adsorbing aqueous Cr(VI), Pb(II) and Cd(II). *Chemosphere* **2021**, *269*, 128409. [CrossRef] [PubMed]
64. Li, Q.; Wang, L.; Xu, R.; Yang, Y.; Yin, H.; Jin, S.; Jiang, T. Potentiality of phosphorus−accumulating organisms biomasses in biosorption of Cd(II), Pb(II), Cu(II) and Zn(II) from aqueous solutions: Behaviors and mechanisms. *Chemosphere* **2022**, *303*, 135095. [CrossRef] [PubMed]
65. Córdova, B.M.; Venâncio, T.; Olivera, M.; Huamani-Palomino, R.G.; Valderrama, A.C. Xanthation of alginate for heavy metal ions removal. Characterization of xanthate-modified alginates and its metal derivatives. *Int. J. Biol. Macromol.* **2021**, *169*, 130–142. [CrossRef]
66. Wang, N.; Wang, M.; Quan, H.; Wang, S.; Chen, D. Waste Camellia oleifera shell-derived hierarchically porous carbon modified by Fe3O4 nanoparticles for capacitive removal of heavy metal ions. *Sep. Purif. Technol.* **2024**, *329*, 125184. [CrossRef]
67. Ma, R.; Feng, Y.; Li, H.; Liu, M.; Cui, Y.; Wang, J.; Shen, K.; Zhang, S.; Tong, S. Deep-sea microorganisms-driven $V^{5+}$and Cd^{2+}removal from vanadium smelting wastewater: Bacterial screening, performance and mechanism. *Environ. Pollut.* **2024**, *360*, 124599. [CrossRef]
68. Jiang, X.; Liu, Z.; Yan, B.; Zhao, L.; Chen, T.; Yang, X. Effects of active silicon amendment on Pb(II)/Cd(II) adsorption: Performance evaluation and mechanism. *J. Hazard. Mater.* **2024**, *478*, 135614. [CrossRef]
69. Wang, H.; Chen, Q.; Xia, H.; Liu, R.; Zhang, Y. Enhanced complexation and electrostatic attraction through fabrication of amino- or hydroxyl-functionalized Fe/Ni-biochar composite for the adsorption of Pb(II) and Cd(II). *Sep. Purif. Technol.* **2024**, *328*, 125074. [CrossRef]
70. Yu, J.; Tong, M.; Sun, X.; Li, B. A simple method to prepare poly(amic acid)-modified biomass for enhancement of lead and cadmium adsorption. *Biochem. Eng. J.* **2007**, *33*, 126–133. [CrossRef]
71. Zhang, C.; Wu, J.; Cao, J. Combined Remediation towards Cadmium–Arsenic-Contaminated Soil via Phytoremediation and Stabilization. *Resources* **2023**, *12*, 109. [CrossRef]
72. Tian, H.; Peng, S.; Zhao, L.; Chen, Y.; Cui, K. Simultaneous adsorption of Cd(II) and degradation of OTC by activated biochar with ferrate: Efficiency and mechanism. *J. Hazard. Mater.* **2023**, *447*, 130711. [CrossRef] [PubMed]
73. Jin, Z.; Xue, Z.; Li, B.; Ou, L.; Yan, L.; Yang, L.; Yin, K.; Jouha, J.; Shao, P.; Zeng, Z.; et al. High-performance spent coffee grounds-based 3D microporous biochar for the efficient capture of Cd^{2+} via a multi-pathway mechanism. *Chem. Eng. J.* **2024**, *485*, 149537. [CrossRef]
74. Wang, N.; Su, Z.; Deng, N.; Qiu, Y.; Ma, L.; Wang, J.; Chen, Y.; Hu, K.; Huang, C.; Xiao, T. Removal of thallium(I) from aqueous solutions using titanate nanomaterials: The performance and the influence of morphology. *Sci. Total Environ.* **2020**, *717*, 137090. [CrossRef] [PubMed]

Disclaimer/Publisher's Note: The statements, opinions and data contained in all publications are solely those of the individual author(s) and contributor(s) and not of MDPI and/or the editor(s). MDPI and/or the editor(s) disclaim responsibility for any injury to people or property resulting from any ideas, methods, instructions or products referred to in the content.